ACS APPLIED MATERIALS & INTERFACES

Research Article

www.acsami.org

Advanced Aromatic Polymers with Excellent Antiatomic Oxygen Performance Derived from Molecular Precursor Strategy and Copolymerization of Polyhedral Oligomeric Silsesquioxane

Pei Wang, Yusheng Tang,* Zhen Yu, Junwei Gu, and Jie Kong*

MOE Key Laboratory of Space Applied Physics and Chemistry, Shaanxi Key Laboratory of Macromolecular Science and Technology, School of Science, Northwestern Polytechnical University, Xi'an 710072, P. R. China

Supporting Information

ABSTRACT: In this contribution, the advanced aromatic polymers with excellent antiatomic oxygen (AO) performance were designed and synthesized using molecular precursor strategy and copolymerization of polyhedral oligomeric silsesquioxane (POSS). A soluble poly(*p*-phenylene benzobisoxazole) (PBO) precursor, that is, TBS−PBO (*tert*-butyldimethylsilyl was denoted as TBS), was designed to overcome the poor solubility of PBO in organic solvents. Then the new copolymer of TBS−PBO−POSS was synthesized by the copolymerization of TBS−PBO and POSS, which possessed good solubility and film-forming ability in common organic solvents, such as *N*-methylpyrrolidone, *N*,*N*-dimethylacetamide, and dimethyl sulfoxide. More importantly, the TBS−PBO−POSS films exhibited outstanding antiatomic oxygen properties because of the incorporation of POSS monomers with cagelike structure into the main chain of copolymer, which drastically reduced the AO-induced erosion owing to the formation of the passivating silica layer on the surface of polymers. When the TBS−PBO−POSS films were exposed to AO effective fluences of 1.5495×10^{20} atom cm^{-2} (5 h) and 4.6486×10^{20} atom cm^{-2} (15 h), the relative mass loss was merely 0.19% and 0.41%, respectively. This work provides a new perspective and efficient strategy for the molecular design of aromatic heterocyclic polymers possessing excellent combination properties including processing convenience and antioxidative and mechanical properties, which can be employed as potential candidates to endure the aggressive environment encountered in low earth orbits.

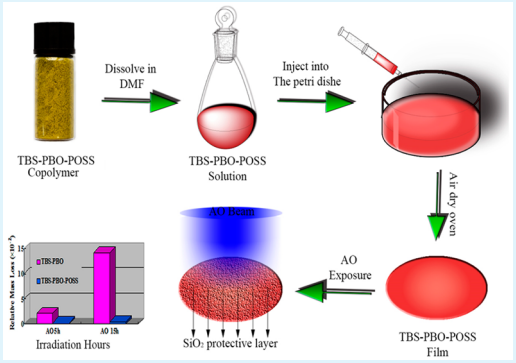

KEYWORDS: *atomic oxygen, aromatic polymers, poly(p-phenylene benzobisoxazole), polyhedral oligomeric silsesquioxnae, molecular precursor*

1. INTRODUCTION

Over the past decades, aromatic heterocyclic polymers have received intensive attention because of their excellent thermal resistance, mechanical performance, and chemical stability.[1,2] Poly(*p*-phenylene benzobisoxazole) (PBO) is one of the important types of aromatic heterocyclic polymers with inherent ladderlike rigid structures and almost the highest thermal stability (decomposition temperature >600 °C).[3−7] However, the application of PBO is often limited because of poor solubility, processing convenience,[8] and ultraviolet radiation resistance.[9] In general, the PBO is insoluble in common organic solvents, which tremendously limits the formation of films, composites, and other desired shapes. Moreover, the PBO is severely eroded upon exposure to multiradiations and atomic oxygen (AO) when being applied in the low earth orbit (LEO) environment.[10−13] Thus, the effective strategy to improve the processing convenience as well as anti-AO property is of significant importance and highly desirable for PBO with outstanding thermal property.[14,15]

Traditionally, the PBO was synthesized via the polycondensation reaction between the 4,6-diaminoresorcinol dihydrochloride (DAR) and terephthalic acid (TPA) or terephthaloyl chloride (TPC) in strong acid solvent with high boiling point such as poly(phosphoric acid) and methanesulfonic acid.[16,17] However, the strong acid was usually difficult to be totally removed, and the residual solvent would severely damage the physical properties of PBO.[18] Fukumaru et al. designed and synthesized soluble precursors of PBO named TBS−PBO via the polycondensation reaction between *tert*-butyldimethylsilyl-functionalized 4,6-diaminoresorcinol (TBS−DAR) and TPC, which exhibited excellent solubility even in common organic solvents including *N*,*N*-dimethylformamide (DMF) and dimethyl sulfoxide (DMSO).[19] The intramolecular cyclization of TBS−PBO at elevated temperatures resulted in the formation of PBO with excellent thermal resistance, mechanical property, and multifunctionalities. Thus, the molecular design of PBO precursors provides a new insight and efficient strategy for improving their processing ability and convenience.

Received: June 20, 2015
Accepted: August 31, 2015
Published: August 31, 2015

DOI: 10.1021/acsami.5b05490
ACS Appl. Mater. Interfaces 2015, 7, 20144−20155

Scheme 1. Schematic Representation of the Synthesis Route of TBS−PBO−POSS from TBS-Functionalized DAR and POSS−Diacylchloride

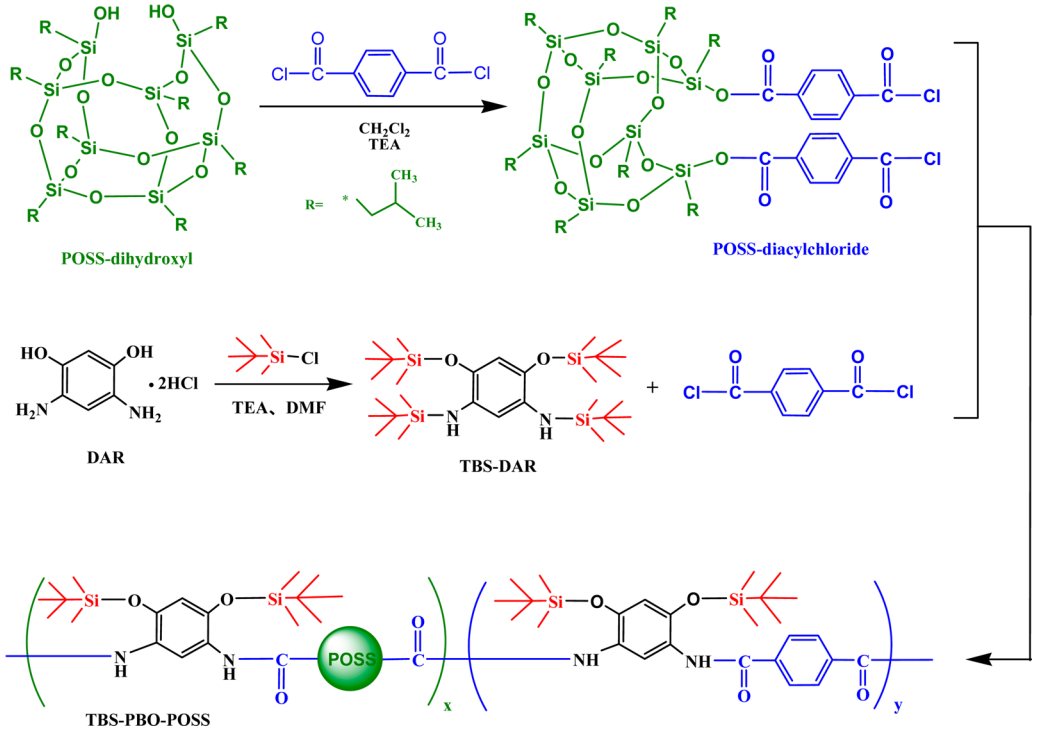

Polyhedral oligomeric silsesquioxanes (POSS) are typical organic−inorganic hybrid materials possessing nanoscaled cube-octameric framework[20] with application in numerous fields, such as thermoset resins, self-assembly, and biomaterials.[21−23] They are the nanostructures with the empirical formula $RSiO_{1.5}$ in which the inorganic silica-like core (Si_8O_{12}) is surrounded by organic corners such as hydrogen, alkyl, aryl, arylene, acrylate, hydroxyl, epoxide, or amino groups.[24−26] The silsesquioxanes include random, ladderlike, cagelike, or partial cage structure. Since POSS are inorganic−organic hybrid network materials with an inner core of inorganic Si−O−Si framework and an outer layer of organic polar or nonpolar constituents, in principle, they have been proved to possess high antioxidative property.[27] It is attributed to the fact that Si−O−Si could first be oxidized leading to the subsequent generation of silica inert protection layers, which protect the inner organic materials from further oxidation and degradation. Therefore, the cagelike POSS with Si−O−Si inorganic−organic framework possess favorable potential application in the environment with multiradiations and high AO.[28−30] In this study, the POSS monomers were incorporated into the main chains of TBS−PBO via copolymerization to obtain soluble TBS−PBO−POSS copolymers with excellent processing convenience and AO-resistant property. It provides a new perspective and efficient strategy for the molecular design of advanced aromatic heterocyclic polymers possessing excellent processing, antioxidative, and mechanical properties with potential in LEOs.

2. RESULTS AND DISCUSSION

2.1. Synthesis of TBS−PBO−POSS Copolymers. The main objective of this study was to produce an efficient TBS−PBO−POSS copolymer via a facile approach, possessing high thermal stability and satisfactory AO resistance. Scheme 1 shows the schematic representation of the synthesis of TBS−PBO−POSS copolymers via a benign condensation reaction of TBS-functionalized DAR (TBS−DAR), TPC, and POSS−diacyl chloride. The detailed polymerization condition is listed in Table 1. The DAR and TPC were employed as starting monomers; however, DAR was easily oxidized and insoluble in common solvents. Herein, we selected TBS as a functional group to obtain TBS-functionalized DAR, which exhibited superior solubility and stability even in air environment.

Table 1. Polymerization Conditions of the Polymer Precursor

	concentration (mmol)			condition		
samples	TBS−DAR	POSS−diacyl chloride	TPC	temperature (°C)	time (h)	solvent
TBS−PBO	1	0	1	r.t.	48	NMP
TBS−PBO−POSS	1	0.1	0.9	r.t.	48	NMP

The TBS−DAR monomer was obtained as a taupe powder. Figure S1a (Supporting Information) shows the characteristic peaks of Si-CH_3 and secondary amine at 1275 and 3400 cm^{-1}, respectively. Moreover, the absence of associated band peaks corresponding to hydroxyl groups and primary amines of DAR monomers at 3200−3500 cm^{-1} suggests the complete protection of the terminal hydroxyls and primary amines by TBS groups. The successful protection of hydroxyls and primary amines by TBS groups resulted in an excellent solubility in $CDCl_3$. Figure 1 shows the ^1H NMR spectrum of TBS−DAR. The protons of TBS group (0.24 and 0.98 ppm), primary amine group (3.68 ppm), and aromatic group (6.24 and 6.28 ppm) can be easily recognized. The ratio of integrated areas of peaks a, b, c, d, and e is

DOI: 10.1021/acsami.5b05490
ACS Appl. Mater. Interfaces 2015, 7, 20144−20155

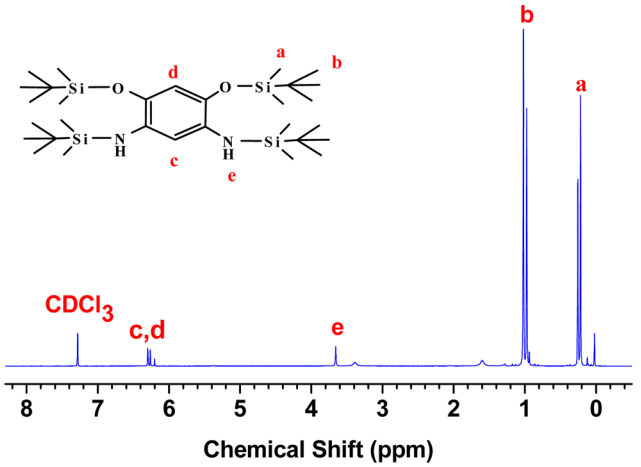

Figure 1. ^{1}H NMR spectrum of TBS−DAR in $CDCl_3$.

24.19:36.34:1.00:1.03:2.01, which is consistent with the expected structural formula of TBS−DAR. It clearly indicates that the hydroxyl groups and primary amine groups of DAR are completely protected by the TBS groups.

Further, the POSS−diacyl chloride for polycondensation was prepared by an esterification reaction between POSS−dihydroxy and excess of TPC in the presence of TEA as an acid-capturer. The products were purified by passing through a silica gel column with dichloromethane as an eluent. POSS−diacyl chloride with acyl chloride and Si−O−C bond was inherently moisture sensitive and kinetically labile, so the fresh POSS−diacyl chloride was used to be reacted after characterization. For POSS−dihydroxy, the FTIR characteristic peaks at ∼3200−3600 cm^{-1} are associated with hydroxyl groups in Figure 2. For the POSS−diacyl chloride, the stretching

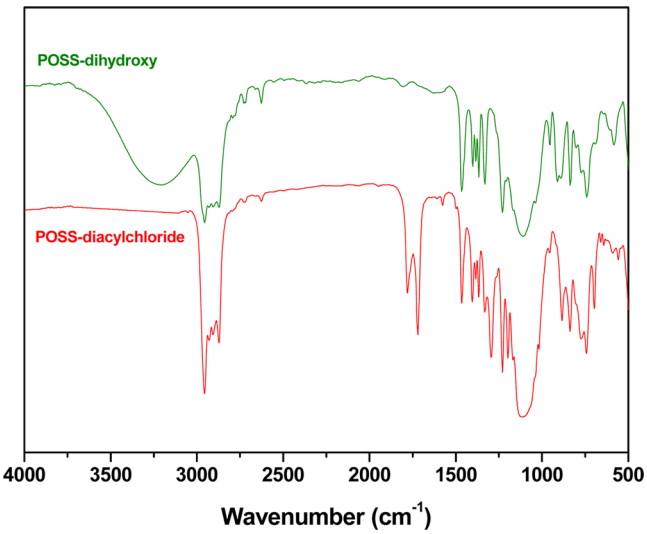

Figure 2. FTIR spectra of POSS−dihydroxy and POSS−diacyl chloride.

vibration peaks of C═O are shifted to low wavenumbers due to the conjugation effect of phenyl groups. Further, the stretching vibration peak corresponding to C═O connected with chlorine appears at 1780 cm^{-1} because of the electron-accepting halogen. Moreover, the C═O peaks connected with oxygen appear at 1720 cm^{-1}. The intense absorption peak at 1080 cm^{-1} confirms the presence of Si−O−Si framework in POSS-containing monomers.[31]

The POSS-containing monomer exhibited a good solubility in $CDCl_3$ to form a homogeneous solution. Figure 3a shows that the resonance peaks observed at 0.66, 0.98, and 1.92 ppm are assigned to peripheral isobutyl groups of POSS monomer, and the ratio of integrated area of peaks a, b, and c is 1.98:6.04:1.00. Simultaneously, the proton peak of the reactive hydroxyl groups (5.08 ppm) is not detected in the NMR spectrum shown in Figure 3b after esterification reaction, suggesting that the modification of dihydroxyl groups was completed. The proton signals at 7.83 and 8.26 ppm are attributed to different chemical environment in benzene, where the ratio of integrated area of peaks c, d, and e is 1.00:0.55:0.48. It is in accordance with the structural formula of POSS−diacyl chloride. In addition, the ^{13}C NMR spectrum of peripheral isobutyl groups of POSS−dihydroxy is shown in Figure S2a. Owing to the effect of hydroxyl group, the -CH_2- peaks of isobutyl groups are splitting into a′ and a (22.6 and 23.2 ppm), which is in correspondence with the -CH_2- groups close to Si−OH and Si−O−Si, respectively. The ratio of integrated areas of peaks a′/a is 1.00:2.96. Since the effect of Si−OH is weak with the extension of alkyl chain, the -CH- and -CH_3- of isobutyl groups have not appeared as the split peaks, and the chemical shifts are at 24.1 and 25.9 ppm. As seen from the ^{13}C NMR spectrum of POSS−diacyl chloride in Figure 3c, the new signals at 131.0, 163.2, and 167.7 ppm are assigned to phenyl −O−C═O and Cl−C═O, respectively, which suggests that the modification of dihydroxyl groups is conducted by TPC.

The ^{29}Si NMR spectrum in Figure S3 also supports the conclusion mentioned above, where the chemical shifts of Si−C═O, Si−O−Si−O, and Si−O−Si−C═O are at −59.0, −66.1, and −67.2 ppm, respectively. As a contrast, the chemical shifts of Si−OH, Si−O−Si−O, and Si−O−Si−OH of starting monomer of POSS−dihydroxyl are at −58.7, −66.7, and −68.6 ppm, respectively (Figure S2b). The above-mentioned results indicated that the TPC was covalently bonded to POSS−dihydroxy. It should be pointed out, since the POSS−diacyl chloride is moisture sensitive, some complex peaks are also observed on the ^{13}C and ^{29}Si NMR spectra. So the POSS−diacyl chloride is directly used to synthesize TBS−PBO−POSS copolymers after preparation.

Subsequently, the soluble TBS−PBO−POSS copolymers were synthesized by the polycondensation reaction between TBS−DAR, POSS−diacyl chloride, and TPC. The so-obtained TBS−PBO−POSS copolymers exhibited excellent solubility in common organic solvents, such as N-methylpyrrolidone (NMP), dimethylacetamide (DMAC), DMF, and DMSO, which provided a convenience for the formation of free-standing films or resin matrix composites. In Figure S1b, the characteristic peaks corresponding to the amide bonds (1610 and 1530 cm^{-1}, C═O stretching mode, and N−H bending mode, respectively) of TBS−PBO and TBS−PBO−POSS are all observed as a result of polycondensation reaction. Further, the characteristic peak at 3420 cm^{-1} is ascribed to the N−H stretching vibration. Moreover, for TBS−PBO−POSS copolymer, the intense absorption peak at 1080 cm^{-1} from Si−O−Si framework confirmed the POSS-containing segments of TBS−PBO−POSS. The ^{1}H NMR spectra of TBS−PBO and TBS−PBO−POSS in DMSO-d_6 are illustrated in Figure 4. The proton at 9.73 ppm is ascribed to N−H (−C═O), which indicates that the polymerization reaction is successfully achieved. Notably, the ^{1}H NMR spectrum of TBS−PBO−

DOI: 10.1021/acsami.5b05490
ACS Appl. Mater. Interfaces 2015, 7, 20144−20155

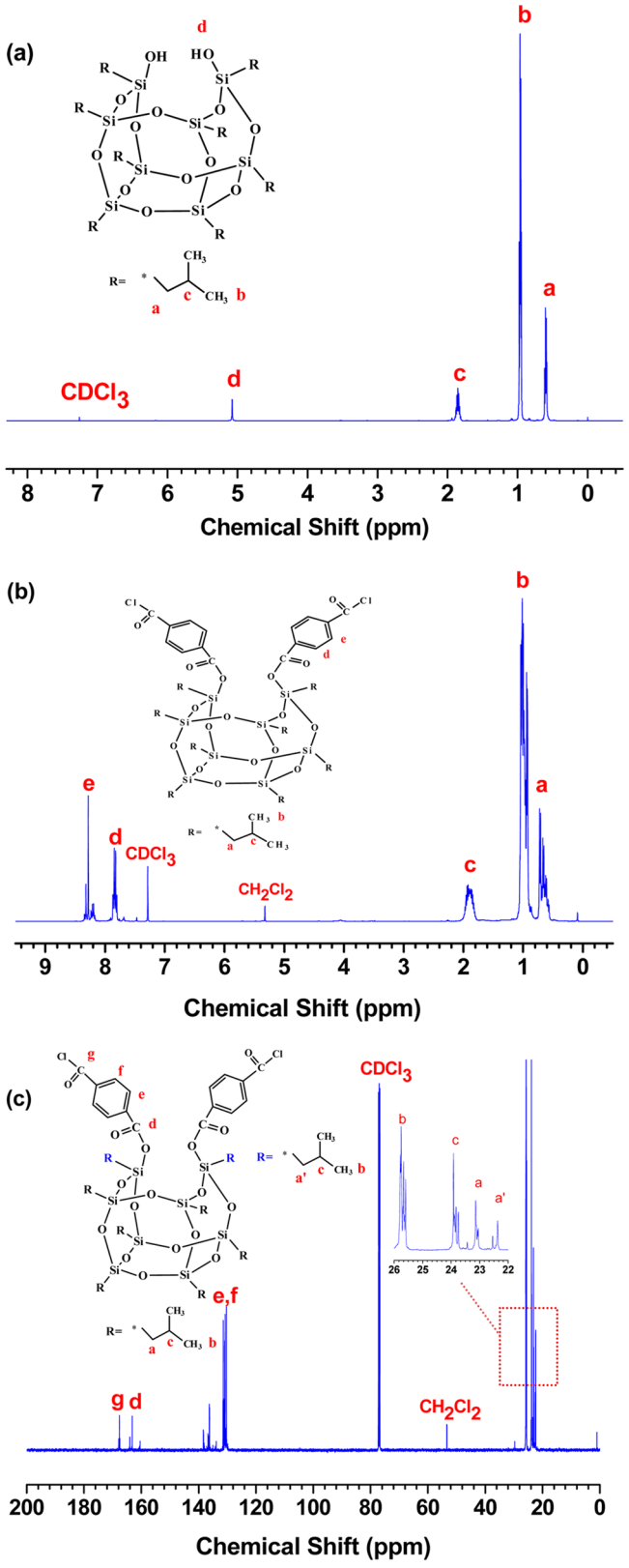

Figure 3. NMR spectra of monomers in $CDCl_3$, (a) ^1H NMR spectrum of POSS−dihydroxy, (b) ^1H NMR spectrum of POSS−diacyl chloride, and (c) ^{13}C NMR spectrum of POSS−diacyl chloride.

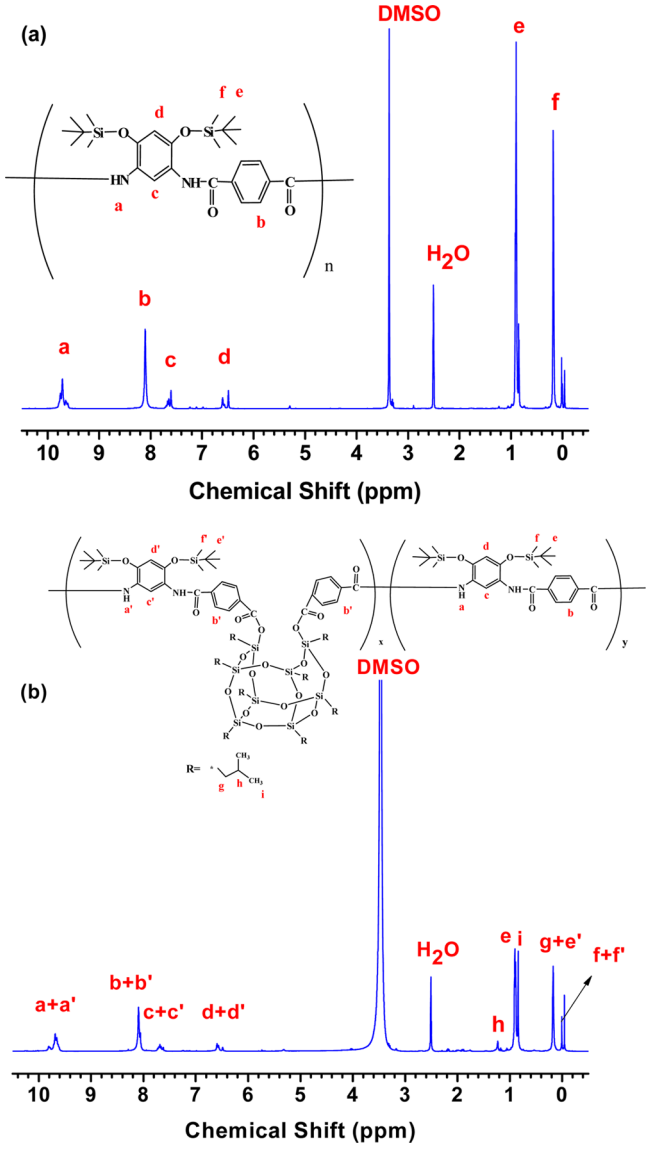

Figure 4. ^1H NMR spectra of (a) TBS−PBO and (b) TBS−PBO−POSS in DMSO-d_6.

POSS (Figure 4b) is similar to that of TBS−PBO (Figure 4a); their resonance peaks are almost at the same chemical shift, and thus the two types of polymers contain similar molecular structures. The difference is observed in the peaks corresponding to the protons of the peripheral isobutyl groups, which are covalently bonded to silicon atoms in TBS−PBO−POSS in Figure 4b. It demonstrates the incorporation of POSS units into the copolymers.

Since the copolymers are strongly absorbed on the chromatographic columns, the molecular weight can not be measured by size exclusion chromatography (DMF−SEC). Herein, their intrinsic viscosity was measured using an Ostwald viscometer in DMF at 30 °C. The intrinsic viscosity of TBS−PBO and TBS−PBO−POSS was 1.03 dL g^{-1} and 0.87 dL g^{-1}, respectively. According the classic Mark−Houwink equation, $[\eta] = KM^{\alpha}$, the intrinsic viscosity of polymers is related with their molecular weight. Owing to the steric hindrance of POSS units, TBS−PBO−POSS copolymer presents a little lower intrinsic viscosity and molecular weight in comparison to TBS−PBO, which both possess film-forming property.

2.2. Anti-AO Erosion Behavior of Copolymer Films. The free-standing TBS−PBO−POSS films with sufficient strength and toughness could easily be obtained via solution

DOI: 10.1021/acsami.5b05490
ACS Appl. Mater. Interfaces 2015, 7, 20144−20155

casting. Thus, the anti-AO erosion measurement could be conveniently performed in the ground-based simulated AO exposure apparatus. The AO possesses strong oxidizing capacity for atoms on materials surface, such as carbon, hydrogen, nitrogen, and silicon. Therefore, it can induce the polymer surface to convert to volatile oxidation products accompanied by an obvious mass loss and roughness of surface. The introduction of POSS segments with Si−O−Si frameworks can form a silica passivation layer under the AO erosion. Since the silica is not sensitive to the oxidation, therefore, the as-generated silica passivation layer can be expected to protect the TBS−PBO−POSS copolymers from further damage from AO erosion.

Figure 5 shows the histogram of the TBS−PBO−POSS films exhibiting good AO resistance. When the TBS−PBO−POSS

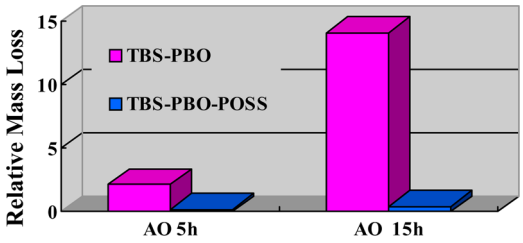

Figure 5. Relative mass loss of TBS−PBO film and TBS−PBO−POSS film when exposed to the AO erosion.

films are exposed to AO effective fluence of 1.5495×10^{20} (5 h) and 4.6486×10^{20} atom cm^{-2} (15 h), the relative mass loss of TBS−PBO−POSS film is merely 0.19% and 0.41%, respectively. However, the mass of TBS−PBO film is decreased dramatically from 2.15% to 14.06%. Notably, after 15 h of AO exposure, the relative mass loss of TBS−PBO−POSS film and TBS−PBO film was ∼2.16 times and 6.54 times as much as that after 5 h of AO exposure. The detailed results of the ground-based simulated experiment are listed in Table 2. It significantly indicates that the POSS content plays an important role in anti-AO erosion when TBS−PBO−POSS film is exposed to AO fluence. As is well-known, the PBO is also sensitive to a long-time ultraviolet (UV) radiation. If the TBS−PBO and TBS−PBO−POSS materials are applied in space environment, the ionizing and UV radiation resistance should be considered. In this ground-based AO exposure measurement, a combined space effect testing facility (CSETF) equipped with neutral AO beam and vacuum ultraviolet ray (VUV) source was employed. Consequently, during the AO exposure process, TBS−PBO and TBS−PBO−POSS films were also etched by VUV, which was an even more abominable circumstance than pure UV irradiation. The results mentioned above suggest that POSS-containing copolymer films also possess a satisfactory performance under a combination of AO beam and UV radiation.

Table 2. AO Erosion Results for TBS−PBO and TBS−PBO−POSS Films before and after Exposure to 5 and 15 h of AO Fluence

samples	AO erosion time (h)	AO fluence (1×10^{20} atom cm^{-2})[a]	m_0 (mg)	m_t (mg)	relative mass loss (1×10^{-2})	RMS (nm)[b]
TBS−PBO	0	0				1.314
	5	1.5495	76.817	75.166	2.1493	17.050
	15	4.6486	75.102	64.546	14.0562	35.519
TBS−PBO−POSS	0	0				2.729
	5	1.5495	67.439	67.309	0.1928	4.608
	15	4.6486	69.340	69.054	0.4112	7.231

[a]AO fluence (F) is the total fluence per unit area of thin film during AO erosion time (t); AO flux (f) is 8.6086×10^{15} atom cm^{-2} s^{-1}, and $F = f \times t$. [b]Root-mean-square roughness values is measured by AFM.

To quantificationally investigate the AO resistance of copolymers, the erosion yield was employed as a relevant parameter for comparison of AO resistance. The erosion yield was defined as shown in Equ.1[32]

$$E = \frac{\Delta m}{A\rho F} \quad (1)$$

where E is the erosion yield (cm^3 $atom^{-1}$), Δm represents the mass loss (g), A is the exposed area (cm^2), ρ denotes the sample's specific gravity (g cm^{-3}), and F is the AO fluence (atoms cm^{-2}). The density of the TBS−PBO film and TBS−PBO−POSS film was 1.213 and 1.089 g cm^{-3}, the exposure area of AO erosion is a circular domain with a diameter of 3.0 cm. The erosion yield of polymer films was calculated, and the detailed results were listed in Table 3. The erosion yield of TBS−PBO−POSS film is much lower than that of TBS−PBO film, suggesting good AO resistance. The low erosion yield was also observed for the various polyimade-based advanced materials.[33,34]The erosion yield of TBS−PBO−POSS film after 15 h of AO erosion was slightly less than that of 5 h. According to the given formula, when the AO erosion duration is increased from 5 to 15 h, the parameters ρ and A are nearly invariant, while F is increased 3 times. With the increase of AO fluence, the $SiO_{1.5}$ frameworks are degraded, and silica-rich protective layers are generated as denoted as SiO_2; the Δm is slowly increased than that of F. So after 15 h of AO exposure, TBS−PBO−POSS film shows unexpected low erosion yield in comparison to TBS−PBO film.

2.3. Surface Morphologies of Copolymer Films. The AO erosion led to etching of materials surface. The field emission scanning electron microscope (FESEM) and atomic force microscope (AFM) observations in Figures 6 and 7 described the surface morphology of TBS−PBO and TBS−PBO−POSS films. Prior to the AO attack, the films are flat and without defect points such as cavities, cracks, and other erosion (Figure 6a,d) with a smaller root-mean-square (RMS) value. However, the Figure 6b,c,e,f shows the appearance of a few cavities when the films are exposed to the AO flux. The surface of TBS−PBO film was significantly influenced in comparison to TBS−PBO−POSS film. Numerous breakdown points were observed on the surface of TBS−PBO film when the AO exposure time was 15 h. However, for the TBS−PBO−POSS film, there were relatively few specks or spots even after 15 h of AO erosion (4.65×10^{20} atom cm^{-2}). Moreover, all the defect points were amplified with the extension in AO erosion time. The surface roughness of the measured samples is increased gradually with the increase of AO flux. In another word, the probability of high-energy AO affecting the surface of films is increased, and AO drastically destroyed the impact sites. These defect points (cavities or microcracks) served as channels for the AO to undercut into the polymer matrix and eventually etch the surfaces.

DOI: 10.1021/acsami.5b05490
ACS Appl. Mater. Interfaces 2015, 7, 20144−20155

Table 3. Erosion Yield of TBS−PBO and TBS−PBO−POSS Films after Exposure to 5 and 15 h of AO Fluence

sample	ρ (g cm^{-3})	A (cm^2)	AO erosion time (h)	F (1×10^{20} atom cm^{-2})	Δm (1×10^{-3} g)	E (1×10^{-25} cm^3 atom^{-1})
TBS−PBO	1.213	7.069	5	1.5495	1.651	12.426
			15	4.6486	10.556	26.482
TBS−PBO−POSS[a]	1.089	7.069	5	1.5495	0.130	1.089
			15	4.6486	0.286	0.799

[a]POSS content was 8.9 wt % in TBS−PBO−POSS film.

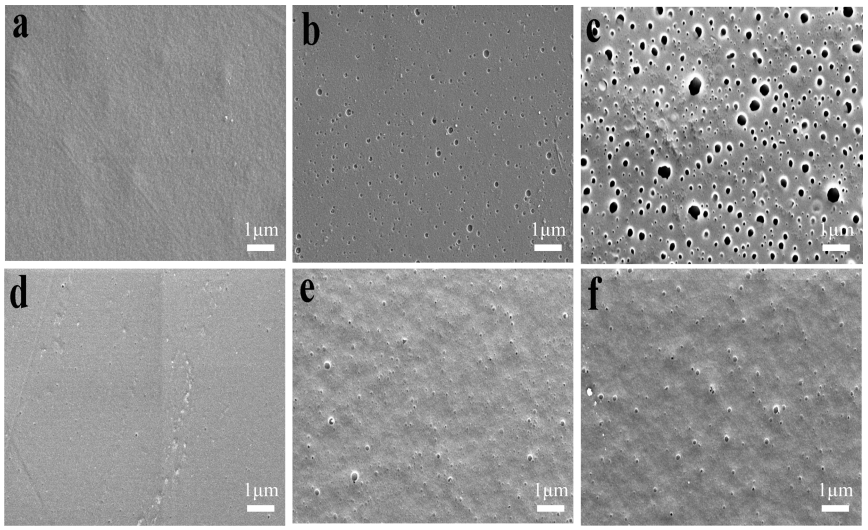

Figure 6. FESEM images of (a−c) TBS−PBO films and (d−f) TBS−PBO−POSS films before and after exposure to 5 and 15 h AO attack, respectively.

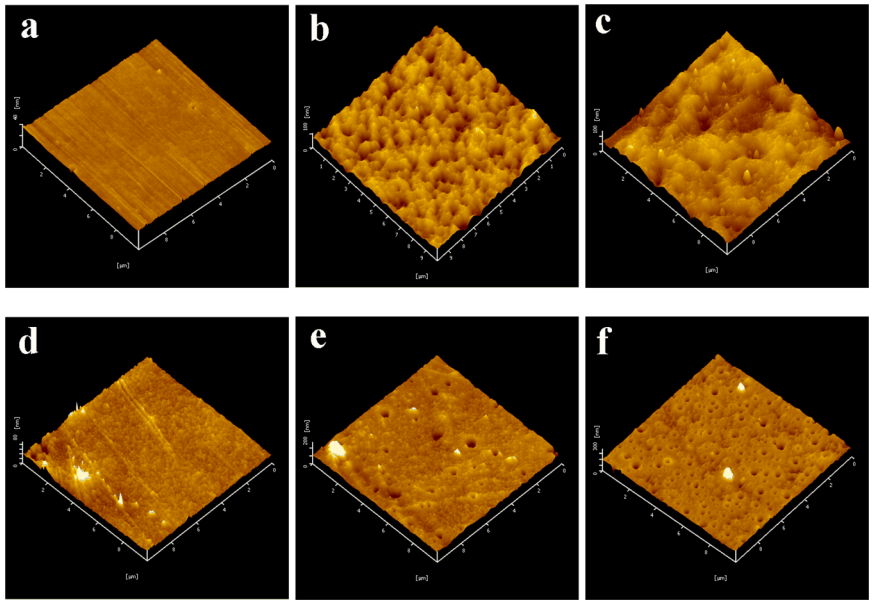

Figure 7. 3D AFM images (10 μm × 10 μm) of (a−c) TBS−PBO films and (d−f) TBS−PBO−POSS films before and after exposure to 5 and 15 h of AO attack, respectively.

Figure 7 shows the three-dimensional (3D) AFM images, where TBS−PBO film becomes dramatically rough and acquires numerous basinlike folds. In contrast, the surfaces of TBS−PBO−POSS films gradually display some short cones with a less extent with an increased AO exposure time. In general, the surface of TBS−PBO−POSS film was much smoother than TBS−PBO film after the same AO erosion time. The RMS value in Table 2 confirms the surface morphologies and surface structures, which are well in agreement with the result of FESEM. In the two-dimensional (2D) AFM images in Figure S4, the AO exposure of 15 h leads to the appearance of a certain amount of defect points such as cavities and breaking points on the surface of TBS−PBO film. However, only a few defect points appear on the surface of TBS−PBO−POSS film besides some SiO_2 particle-like structure. The silica-rich layer

DOI: 10.1021/acsami.5b05490
ACS Appl. Mater. Interfaces 2015, 7, 20144−20155

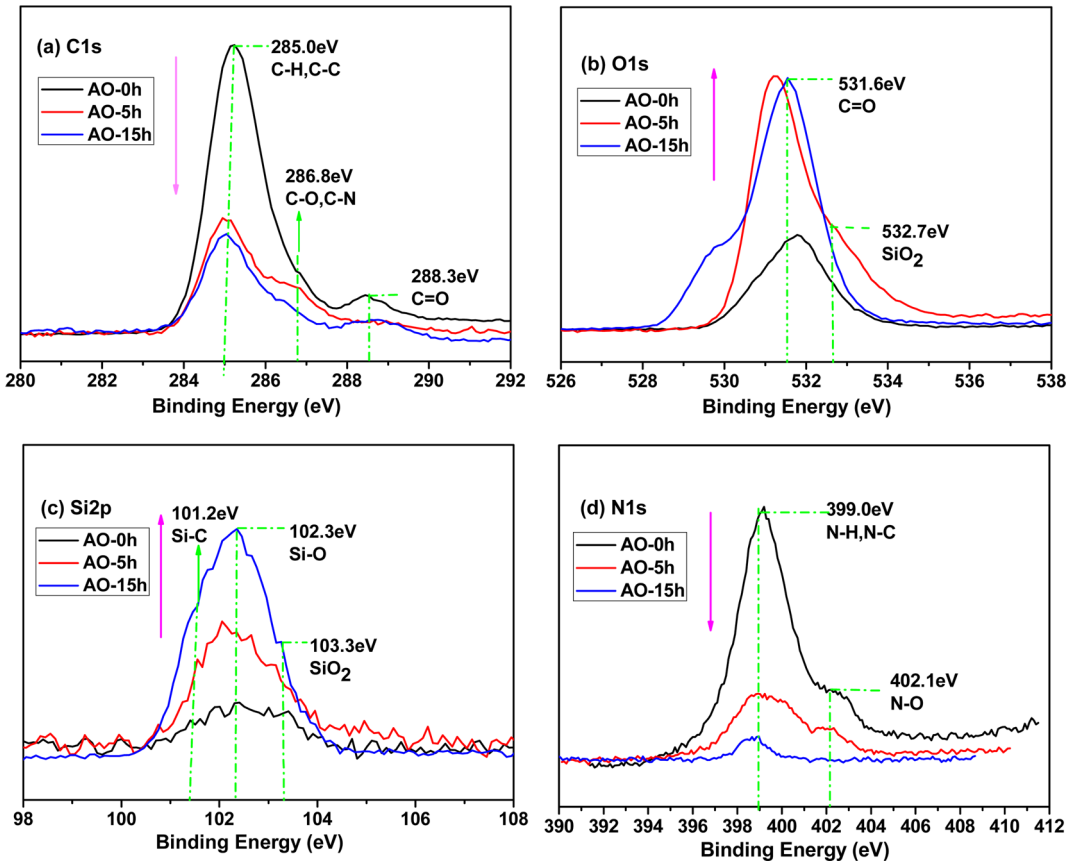

Figure 8. High-resolution XPS spectra of TBS−PBO films: (a) C 1s, (b) O 1s, (c) Si 2p, and (d) N 1s before and after AO exposure with total AO fluence of 1.5495×10^{20} (5 h) and 4.6486×10^{20} atom cm^{-2} (15 h).

was ascribed to the generation of SiO_2 passivation layer during the AO etch process.[35]

2.4. X-ray Photoelectron Spectroscopy Analyses of Copolymer Films. The surface nature and chemical component of TBS−PBO−POSS films after AO exposure were investigated via X-ray photoelectron spectroscopy (XPS). In Figures 8 and 9, the films exhibit carbon, oxygen, silicon, and nitrogen on the surface, where the atomic concentration is presented in Table 4. The atomic ratio of TBS−PBO and TBS−PBO−POSS prior to AO erosion is in correspondence with the theoretical calculation of polymers. The strong oxidizing AO could be reacted with the polymer surface atoms such as carbon, hydrogen, nitrogen, and silicon; therefore, some of these atoms are transformed to volatile gases, and the concentration of carbon and nitrogen is decreased significantly on surface. During the AO exposure process, the formed silicon dioxide and other oxides generated were nonvolatile, so the concentration of oxygen and silicon is increased on surface.

In detail, the XPS spectra of TBS−PBO film before and after AO exposure are shown in Figure 8. The concentration of carbon atoms is decreased significantly; however, the concentration of oxygen atom is increased to some extent with the increase of AO exposure time. In Figure 8a, the intensity of peaks at 285.0 eV (C−H, C−C), 286.8 eV (C−O, C−N), and 288.3 eV (C═O) is all decreased with the increase of AO exposure time. In particular, the peaks of C−H or C−C at 285.0 eV demonstrate that the alkyl groups of TBS−PBO polymer were predominantly broken by the AO irradiation.[36,37] Furthermore, the peak at 531.6 eV in O 1s, 102.3 eV in Si 2p, and 399.0 eV in N 1s was assigned to C═O, Si−O, N−H, and N−C, respectively.[38] The relative intensity of peaks and shoulders were changed slightly when the film was exposed to AO fluence. It was related to the change in chemical environment of atoms on surface. When the AO exposure time is increased from 5 to 15 h, the atom concentration of TBS−PBO film is changed significantly. The extension in AO erosion time results in a decrease in the exposed carbon or nitrogen atoms and a reduction in the concentration of absorbable AO fluence with reduced antioxidizing ability.[39]

For the TBS−PBO−POSS film, the significant difference is the O 1s signal as shown in Figure 9b. In a long AO erosion time, the $RSiO_{1.5}$ at 531.6 eV was oxidized and transformed to high oxidation state of SiO_2. Simultaneously, the shape of the spectra is also changed with respect to that before AO erosion. It is confirmed by the relative increase in intensity of SiO_2 at 532.7 eV,[40] which indicates that the cagelike POSS units with Si−O−Si frameworks in copolymer are more effective in the formation of SiO_2 layer during the AO corrosion. Under the protection silica layers, the long AO exposure time (15 h) leads to a significant decrease in the concentration of carbon and nitrogen atoms to a lower level. Accordingly, the TBS−PBO−POSS films show excellent anti-AO properties as described above.

2.5. Thermal Properties of Copolymer Films. Figure 10a shows the air-atmosphere thermogravimetric analysis (TGA) curves. For the pure POSS−dihydroxy, the initial sublimation or decomoposition temperature is 230 °C, which is followed by an extremely rapid sublimation and thermolytic degradation in the range of 230−400 °C. Subsequently, the TGA curve forms

DOI: 10.1021/acsami.5b05490
ACS Appl. Mater. Interfaces 2015, 7, 20144−20155

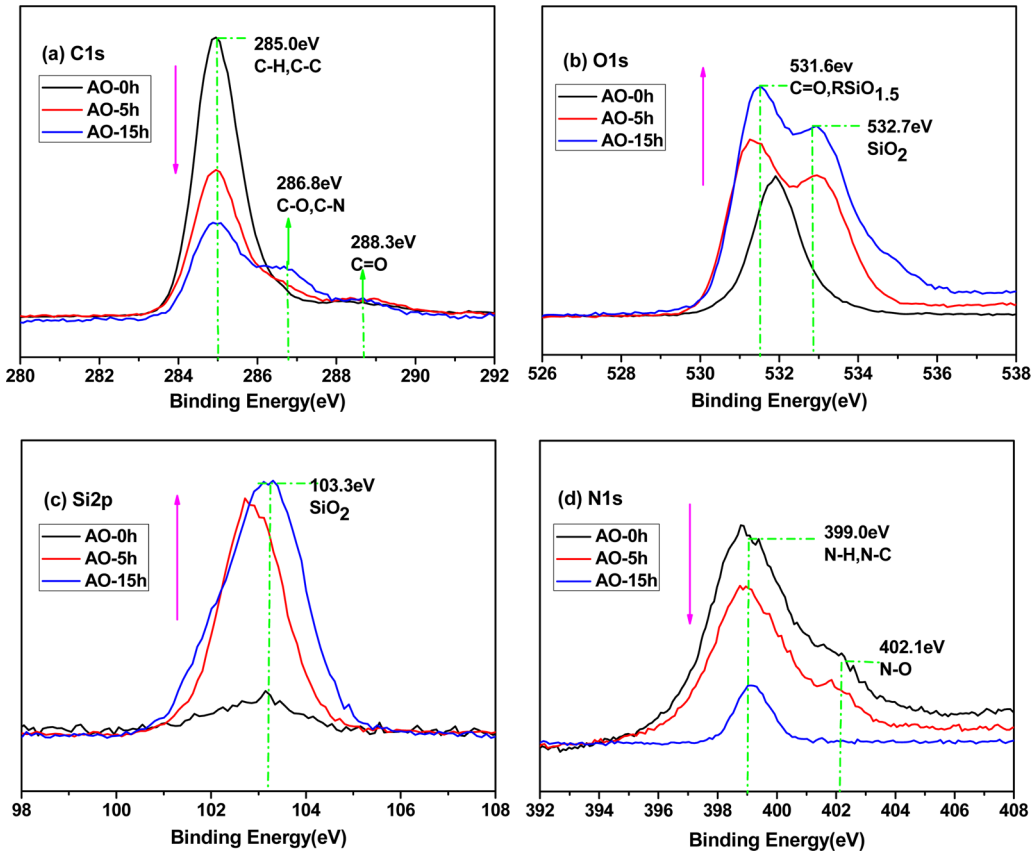

Figure 9. High-resolution XPS spectra of TBS−PBO−POSS films: (a) C 1s, (b) O 1s, (c) Si 2p, and (d) N 1s before and after AO exposure with total AO fluence 1.5495×10^{20} (5 h) and 4.6486×10^{20} atom cm^{-2} (15 h).

Table 4. Surface Atomic Concentrations (%) of TBS−PBO and TBS−PBO−POSS Films before and after 5 and 15 h of AO Erosion

samples	AO erosion time (h)	C 1s (%)	O 1s (%)	Si 2p (%)	N 1s (%)
TBS−PBO	0	76.40	11.82	5.83	5.85
	5	49.12	29.89	17.16	2.64
	15	46.13	31.79	18.93	1.73
TBS−PBO−POSS	0	74.26	13.81	6.97	4.95
	5	59.28	21.47	16.69	2.17
	15	46.52	33.15	19.21	1.03

a platform at 55% in the range of 400−750 °C. For the TBS−PBO and TBS−PBO−POSS, The intramolecular cyclization at 300 °C leads to the formation of oxazole rings on the main chain of PBO and PBO−POSS, which provide thermal resistance in argon atmosphere higher than 350 and 650 °C as shown in Figure 10b, respectively. Notice that, in argon atmosphere, the PBO−POSS film exhibited lower thermal stability than PBO film. However, in an air atmosphere (O_2/N_2 = 20/80, v/v), the PBO−POSS shows almost the same thermal stability with PBO film. They both start to be thermolytically degraded from 350 °C and show an extremely rapid thermolytic degradation in the temperature range of 550−700 °C because of the strong oxidation. In comparison to PBO, the results demonstrate that the PBO−POSS is more stable in oxygen-containing atmosphere owing to cagelike Si−O−Si frameworks.

In the LEO circumstance, the space effect on materials is very severe and complex because of the synergistic interaction of orbital environments such as high-energy radiation particles, atomic oxygen, micrometeoroids, orbital debris, and ultraviolet irradiation interacting synergistically, along with thermal exposure.[41] It was reported that AO fluence in LEO was from 1×10^{12} to $\sim 1 \times 10^{15}$ atom cm^{-2} s^{-1}, and exposure of 2.0×10^{20} atom cm^{-2} was roughly equivalent to 6 months exposure to AO in an LEO circumstance.[34] The polyimide films were exposed to atomic oxygen in the space environment on the Materials International Space Station Experiment (MISSE) platform. The flight experiment was retrieved after 3.9 years. The samples were exposed to the ram and therefore all components of the LEO environment, including atomic oxygen and vacuum ultraviolet light, with the AO fluence of $\sim 8 \times 10^{21}$ atom cm^{-2}. When the free-standing films of polyimide reach to a Kapton blanket and are exposed to a sweeping ram (a variety of incidence angles) in LEO on MISSE-5 for ca. one year, the AO fluence is estimated to be 1.8×10^{20} atom cm^{-2}.[42] So the duration of materials in LEO environment can be approximately predicted based on AO fluence, although there is no linear relationship. For these TBS−PBO−POSS copolymers, the AO exposure of 15 h (4.6486×10^{20} atom cm^{-2}) amounts to ca. two years in LEO environment.

2.6. Mechanical Properties of Copolymer Films. As is well-known,[43,44] the thorough dispersion of POSS into polymer matrix could obviously improve mechanical properties of composites. Therefore, in this study, the mechanical properties including the Young's modulus, tensile strength, and ultimate strain of TBS−PBO−POSS and TBS−PBO films were

DOI: 10.1021/acsami.5b05490
ACS Appl. Mater. Interfaces 2015, 7, 20144−20155

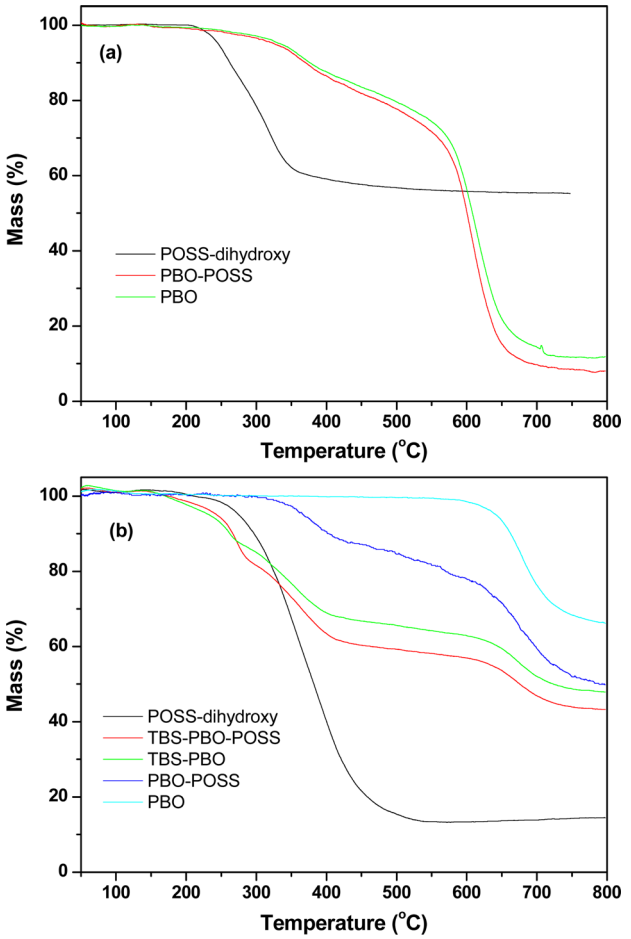

Figure 10. TGA curves of (a) POSS−dihydroxy, PBO−POSS copolymer, and PBO at a heating rate of 10 °C min^{-1} under air flow; (b) POSS−dihydroxy, TBS−PBO polymer, PBO, TBS−PBO−POSS copolymer, and PBO−POSS at a heating rate of 10 °C min^{-1} under argon flow.

investigated as listed in Table 5 to observe the influence of AO exposure.

Table 5. Mechanical Properties of TBS−PBO and TBS−PBO−POSS Films before and after 5 and 15 h of AO Exposure

samples	AO erosion time (h)	Young's modulus (GPa)	tensile strength (MPa)	elongation at break (%)
TBS−PBO	0	2.72	4.90	0.18
	5	1.69	6.24	0.37
	15	1.45	8.27	0.57
TBS−PBO−POSS	0	8.37	26.77	0.32
	5	6.34	36.13	0.57
	15	3.92	15.17	0.38

Figure 11 and Table 5 show that the tensile strength and elongation at break of the TBS−PBO films are relatively poor and improve slightly with the increase in AO erosion time. In contrast, the TBS−PBO−POSS films exhibit a much better tensile strength than TBS−PBO films either before or after AO exposure. The incorporation of cagelike POSS units in copolymer main chains significantly improves the mechanical

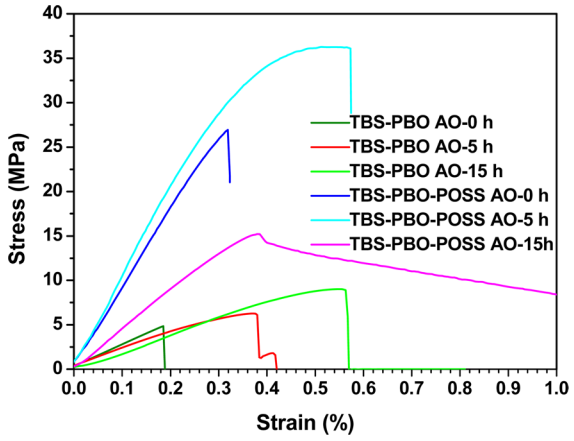

Figure 11. Selective representation of stress−strain curves of TBS−PBO films and TBS−PBO−POSS films before and after exposure to 5 and 15 h of AO erosion.

properties. The tensile strength of TBS−PBO film and TBS−PBO−POSS film prior to AO erosion is 4.90 and 26.77 MPa, respectively, and the elongation at break also increased from 0.18 to 0.32%, which indicates that the ductility of TBS−PBO−POSS film is improved due to the introduction of POSS units. The low elongation at break of TBS−PBO and TBS−PBO−POSS films is ascribed to the stiff rigid structure of PBO. However, under the AO exposure, the tensile strength and elongation at break of TBS−PBO−POSS film are both increased. The maximum tensile strength and elongation at break is 36.13 MPa and 0.57%, respectively. The bulky spheroid and cagelike structure of POSS units may enhance the interval between the PBO matrix, which resulted in the increase in free volume of the copolymers.[45,46] The tension stress in TBS−PBO−POSS film leads to the uniform dispersion of the energy to cagelike Si−O−Si frameworks. Under the AO exposure, the regular structure of TBS−PBO−POSS copolymer is further destroyed, and the poor interaction is helpful to increase the ductility and toughness of copolymer films to some extent.[34]

3. CONCLUSIONS

A novel and facile synthetic strategy was established to obtain soluble and film-forming TBS−PBO−POSS copolymers via polycondensation reaction of TBS-functionalized monomers. The TBS−PBO−POSS films exhibited outstanding anti-AO property because of the incorporation of POSS units with cagelike structure into the main chain of PBO. When the TBS−PBO−POSS films were exposed to AO fluences of 1.5495×10^{20} atom cm^{-2} (5 h) and 4.6486×10^{20} atom cm^{-2} (15 h), the relative mass losses were merely 0.192 and 0.411%, respectively. Accordingly, the erosion yield is obviously decreased. Furthermore, the POSS units presented an effective reinforcement toward the matrix, and the ductility for TBS−PBO−POSS films before and after AO exposure was higher than that of TBS−PBO films. This study provides an efficient strategy and important fundamental results for the molecular design of aromatic heterocyclic polymers possessing excellent processing, antioxidative, and mechanical properties, which are potential candidates to endure the aggressive environment encountered in LEOs.

DOI: 10.1021/acsami.5b05490
ACS Appl. Mater. Interfaces 2015, 7, 20144−20155

4. EXPERIMENTAL SECTION

4.1. Materials. *tert*-Butyldimethylsilyl chloride (TBS), 4,6-diaminoresorcinol dihydrochloride (DAR), and terephthaloyl chloride (TPC) were purchased from TCI Shanghai Chem. Industry Co., Ltd. (China). 1,3,5,7,9,11-octaisobutyltetracyclo (POSS−dihydroxy) was purchased from Hybrid Plastics Inc. (USA) and used as received. Triethylamine (TEA) was purchased from J&K Scientific Ltd. (China) and purified by distillation over potassium hydroxide. Dichloromethane (DCM), *N*-methylpyrrolidone (NMP), *N*,*N*-dimethylformamide (DMF), and silica gel (70−230 mesh) were purchased from Alfa Aesar (China). TPC was purified by recrystallization from *n*-hexane, and the other reagents were used as received without further purification.

4.2. Synthesis. *4.2.1. Synthesis of 4,6-Di(tert-butyldimethylsilylamino)-1,3-di(tert-butyldimethylsiloxy)-benzene (TBS−DAR).* DAR (2.13 g, 10 mmol) and anhydrous DMF (50 mL) under argon atmosphere were added into a 250 mL anhydrous and anaerobic Schlenk flask equipped with a magnetic stirring bar and an argon inlet. *tert*-Butyldimethylsilyl chloride (15 g, 100 mmol) was dissolved in anhydrous DMF (50 mL). Subsequently, TBS solution and TEA (27.3 g, 270 mmol) were simultaneously charged dropwise into the above-mentioned reaction mixture with continuous stirring to form slurry. The mixture was allowed to react under stirring at ambient temperature (r.t.) for 24 h to produce precipitates. Following the completion of the reaction, the mixture was filtered and then rinsed several times with deionized water. The obtained solid was dried at 80 °C for 24 h in a vacuum oven to obtain a cinereous powder (5.23 g, 87.6%). ^{1}H NMR (400 MHz, $CDCl_3$, δ): 6.28 (1H, Ar−H), 6.24 (1H, Ar−H), 3.68 (2H, N−H), 0.98 (36H, $(CH_3)_3$), 0.24 (24H, $Si(CH_3)_2$).

4.2.2. Synthesis of POSS−Diacyl Chloride. A dry and argon-flushed 100 mL anaerobic Schlenk flask equipped with a magnetic stirring bar and an argon inlet was charged with TPC (2.51 g, 12.36 mmol) and anhydrous DCM (20 mL). POSS−dihydroxy (5.0 g, 5.61 mmol) was dissolved in 20 mL of anhydrous DCM. Subsequently, POSS-containing solution and TEA (1.25 g, 12.36 mmol) were simultaneously added dropwise into the reaction vessel under stirring in an ice−water bath. The mixture was stirred at r.t. for 24 h. The crude product was passed through a silica gel column with dichloromethane as eluent, and the fractions were rotary-evaporated to obtain white fatty solids (5.63 g, 82%). ^{1}H NMR (400 MHz, $CDCl_3$, δ): 8.26 (4H, Ar−H), 7.83 (4H, Ar−H), 1.92 (8H, C−H), 0.98 (48H,$(CH_3)_2$), 0.66 (16H, CH_2).

4.2.3. Synthesis of TBS−PBO−POSS Copolymers. The polymerization was performed in an argon-filled Schlenk tube by the following general procedure: TBS−DAR (0.597 g, 1.0 mmol) was dissolved in NMP (2 mL) and then cooled to 0 °C, following which POSS−diacyl chloride (0.1225 g, 0.1 mmol) and TPC (0.183 g, 0.9 mmol) were added. The solution became moderately viscous and was stirred at r.t. for 48 h. After the completion of the reaction, the solution was added into 200 mL of deionized water to produce a precipitate, which was filtered and rinsed several times with water. The obtained solid was dried at 80 °C for 24 h in a vacuum oven that afforded a brown powder (0.47 g, 78%). The molar ratio of monomers was 1:0.1:0.9, and the synthetic copolymer was denoted as TBS−PBO−POSS. In this study, we mainly focused on two types of polymers for the comparison purposes. The other polymer (TBS−PBO) was prepared in accordance with the above-mentioned method, and the polymerization conditions are listed in Table 1.

4.2.4. Fabrication of Free-Standing Copolymer Films. The solution of synthesized TBS−PBO−POSS (100 mg) or TBS−PBO (100 mg) in DMF (2 mL) filtered through a filter with a diameter of 0.22 μm was casted on a dust-free glass plate and immediately placed in an air-circulation oven at 80 °C for 4 h, respectively. An amber and visibly tough film was formed. The film was peeled off the glass substrate by immersing the substrate in deionized water. The residual organic solvent and water were removed at 80 °C for 12 h in a vacuum oven, and the round films with diameters of 3.0 cm were sealed for measurement and testing.

4.3. Characterization. Fourier transform infrared spectroscopy (FTIR) measurement was performed using a Nicolet iS10 IR spectrometer. FTIR spectrometer was operated at r.t. in the range of 4000−500 cm^{-1} with a resolution of 2 cm^{-1} and 16 scans. Powder samples were prepared by dispersing the samples in KBr and compressing the mixture to form disks. Nuclear magnetic resonance (NMR) spectra were recorded in $CDCl_3$ with tetramethylsilane (TMS) as internal standard for ^{1}H NMR and ^{13}C NMR, using a Bruker Avance 400 spectrometer (400 MHz, Bruker BioSpin, Switzerland). ^{29}Si NMR spectra were recorded on a Bruker Avance 500 spectrometer (Bruker BioSpin, Switzerland) operating at 50.7 MHz in $CDCl_3$. Chemical shifts are referenced to TMS. Intrinsic viscosity measurement was performed on an Ostwald viscometer with the capillary inner diameter of 6 mm.

Field emission scanning electron microscopy (FESEM) analysis was performed using a ZEISS SUPRA 55 Instrument (Carl Zeiss Jena, Germany). The sample was sputtered with a thin layer of gold (1 to 2 mm) prior to each measurement. Atomic force microscopy (AFM) analysis and RMS roughness values were obtained using an SPI3800-SPA-400 (Japan, NSK Ltd.) scanning force microscope in tapping mode equipped with Olympus cantilevers (spring constant is 1.6 N m^{-1}) under ambient conditions.

X-ray photoelectron spectroscopy (XPS) measurement was conducted using a Kα spectrometer (Axis Ultra, Kratos Analytical Ltd., U.K.), and the core level spectra were measured using a monochromatic Al Kα X-ray source ($h\nu$ = 1486.7 eV). The analyzer was operated at 23.5 eV pass energy, and the analyzed area was 200−800 μm in diameter. The lowest energy resolution was 0.48 eV (Ag $3d_{5/2}$). Binding energies were referenced to the adventitious hydrocarbon C 1s line at 285.0 eV, and the curve fitting of the XPS spectra was performed using the least-squares method. Thermogravimetric analysis (TGA) was performed using a thermoanalyzer STA 449 F3 (Netzsch Group, Germany) in a temperature range of 40−1200 °C, with a heating rate of 10 K min^{-1} in an argon or air atmosphere (a gas flow of 50 mL min^{-1}). Stress−strain curve was measured using Instron OP336−43 instrument (Instron Corporation, US) at r.t. with a crosshead speed of 5 mm min^{-1}.

The ground-based simulated AO exposure experiment was performed with a combined space effect testing facility (CSETF) equipped with neutral AO beam and vacuum ultraviolet ray (VUV) source.[11,39,47] Atomic oxygen was emitted by a microwave electron cyclotron resonance (ECR) with a dominating section for the ECR-AB200 plasma AO production instrument. The ECR oxygen neutral beam source was operated at 3 kV and 55 mA to emit the microwaves, and the oxygen molecules were dissociated and ionized into the oxygen plasma. The oxygen plasma mainly includes neutral O atoms, electrons, O_2^+, O^+, and molecular oxygen (ionic component <0.1%). The mole fraction of atomic oxygen in the beam was above 90%. The AO flux in the system was finally calibrated to be 8.6086×10^{15} atom cm^{-2} s^{-1}. The translational energy of AO was 3.0−10.0 eV. The neutral AO beam had a peak energy of ∼7 eV, with a full width at half-maximum in the distribution of ±3 eV. The AO equivalent fluence measurement was calibrated based on 50 μm thick Kapton H film (DuPont, Inc.) mass loss, assuming an erosion yield of 3.0×10^{-24} cm^3 $atom^{-19}$. The mass loss of test films was determined by using an analytical balance (HEG42−120200−7), which was a combined device for ECR-AB200 plasma atomic oxygen production instrument with an accuracy of ±1 μg.[48] All the polymer films were kept in a vacuum oven at 80 °C for 12 h to ensure the complete removal of water and residual solvents prior to the measurement.

■ ASSOCIATED CONTENT

Supporting Information

The Supporting Information is available free of charge on the ACS Publications website at DOI: 10.1021/acsami.5b05490.

FTIR and NMR spectra of monomers and polymers. (PDF)

DOI: 10.1021/acsami.5b05490
ACS Appl. Mater. Interfaces 2015, 7, 20144−20155

AUTHOR INFORMATION

Corresponding Authors

*E-mail: kongjie@nwpu.edu.cn. Phone (fax): +86-29-88431621. (J.K.)

*E-mail: tys@nwpu.edu.cn. Phone (fax): +86-29-88493700. (Y.T.)

Notes

The authors declare no competing financial interest.

ACKNOWLEDGMENTS

The financial support from the Key Project of Aerospace Technology Innovation Foundation and the Fundamental Research Funds for the Central Universities is acknowledged. J.K. is thankful for the grant from the Program of New Century Excellent Talents of Ministry of Education of China (NCET-11-0817).

REFERENCES

(1) Wei, J.; Zhang, S.; Liu, X. Y.; Qian, J.; Hua, J. S.; Li, X. X.; Zhuang, Q. X. In situ Synthesis of Ternary $BaTiO_3$/MWNT/PBO Electromagnetic Microwave Absorption Composites with Excellent Mechanical Properties and Thermostabilities. *J. Mater. Chem. A* **2015**, *3*, 8205−8214.

(2) Arnold, F. E.; Van Deusen, R. L. Unusual Film-forming Properties of Aromatic Heterocyclic Ladder Polymers. *J. Appl. Polym. Sci.* **1971**, *15*, 2035−2047.

(3) Fukumaru, T.; Saegusa, Y.; Fujigaya, T.; Nakashima, N. Fabrication of Poly(p-phenylenebenzobisoxazole) Film using a Soluble Poly(o-alkoxyphenylamide) as the Precursor. *Macromolecules* **2014**, *47*, 2088−2095.

(4) Lee, J. K.; Kim, J. H.; Kim, Y. J. Synthesis and Characterization of Fluorine-containing Polybenzoxazoles by High-temperature Direct Polycondensation. *Bull. Korean Chem. Soc.* **2003**, *24*, 1029−1031.

(5) Matsuura, T.; Ando, S.; Matsui, S.; Sasaki, S.; Yamamoto, F. Heat-resistant Singlemode Optical Waveguides using Fluorinated Polyimides. *Electron. Lett.* **1993**, *29*, 2107−2109.

(6) Cheng, S. Z. D.; Wu, Z. Q.; Mark, E.; Hsu, S. L. C.; Harris, F. W. A High-performance Aromatic Polyimide Fibre: 1. Structure, Properties and Mechanical-history Dependence. *Polymer* **1991**, *32*, 1803−1810.

(7) Su, P. H.; Cheng, J.; Li, J. F.; Liao, Y. H.; Yu, T. L. High Temperature Polybenzimidazole Membrane Electrode Assemblies using Pyridine-polybenzimizazole as Catalyst Layer Binder. *J. Power Sources* **2014**, *260*, 131−139.

(8) So, Y. H.; Bell, B.; Heeschen, J. P.; Nyquist, R. A.; Murlick, C. L. Poly(p-phenylenebenzobisoxazole) Fiber with Polyphenylene Sulfide Pendent Groups. *J. Polym. Sci., Part A: Polym. Chem.* **1995**, *33*, 159−164.

(9) Zhang, C. H.; Huang, Y. D.; Yuan, W. J.; Zhang, J. N. UV Aging Resistance Properties of PBO Fiber Coated with Nano-ZnO Hybrid Sizing. *J. Appl. Polym. Sci.* **2011**, *120*, 2468−2476.

(10) Koontz, S. L.; Leger, L. J.; Visentine, J. T.; Hunton, D. E.; Cross, J. B.; Hakes, C. L. EOIM-III Mass Spectrometry and Polymer Chemistry-STS 46. *J. Spacecr. Rockets* **1995**, *32*, 483−495.

(11) Buczala, D. M.; Brunsvold, A. L.; Minton, T. K. Erosion of Kapton H by Hyperthermal Atomic Oxygen. *J. Spacecr. Rockets* **2006**, *43*, 421−425.

(12) Waters, D. L.; Banks, B. A.; De Groh, K. K.; Miller, S. K. R.; Thorson, S. D. The Atomic Oxygen Erosion Depth and Cone Height of Various Materials at Hyperthermal Energy. *High Perform. Polym.* **2008**, *20*, 512−522.

(13) Nicholson, K. T.; Sibener, S. J.; Minton, T. K. Nucleation and Growth of Nanoscale to Microscale Cylindrical Pits in Highly-ordered Pyrolytic Graphite upon Hyperthermal Atomic Oxygen Exposure. *High Perform. Polym.* **2004**, *16*, 197−206.

(14) Zhang, K.; Liu, J.; Ohashi, S.; Liu, X.; Han, Z.; Ishida, H. Synthesis of High Thermal Stability Polybenzoxazoles via Ortho-imide-functional Benzoxazine Monomers. *J. Polym. Sci., Part A: Polym. Chem.* **2015**, *53*, 1330−1338.

(15) Chen, L.; Wei, F.; Liu, L.; Cheng, W. L.; Hu, Z.; Wu, G. S.; Du, Y. Z.; Zhang, C. H.; Huang, Y. D. Grafting of Silane and Graphene Oxide onto PBO Fibers: Multifunctional Interphase for Fiber/polymer Matrix Composites with Simultaneously Improved Interfacial and Atomic Oxygen Resistant Properties. *Compos. Sci. Technol.* **2015**, *106*, 32−38.

(16) Wolfe, J. F.; Arnold, F. E. Rigid-rod Polymers. 1. Synthesis and Thermal Properties of Para-aromatic Polymers with 2, 6-Benzobisoxazole Units in the Main Chain. *Macromolecules* **1981**, *14*, 909−915.

(17) Choe, E. W.; Kim, S. N. Synthesis, Spinning, and Fiber Mechanical Properties of Poly (p-phenylenebenzobisoxazole). *Macromolecules* **1981**, *14*, 920−924.

(18) Walsh, P. J.; Hu, X. B.; Cunniff, P.; Lesser, A. J. Environmental Effects on Poly-p-phenylenebenzobisoxazole Fibers. I. Mechanisms of Degradation. *J. Appl. Polym. Sci.* **2006**, *102*, 3517−3525.

(19) Fukumaru, T.; Fujigaya, T.; Nakashima, N. Extremely High Thermal Resistive Poly (p-phenylene benzobisoxazole) with Desired Shape and Form from a Newly Synthesized Soluble Precursor. *Macromolecules* **2012**, *45*, 4247−4253.

(20) Kannan, R. Y.; Salacinski, H. J.; Butler, P. E.; Seifalian, A. M. Polyhedral Oligomeric Silsesquioxane Nanocomposites: the Next Generation Material for Biomedical Applications. *Acc. Chem. Res.* **2005**, *38*, 879−884.

(21) Lin, Z. W.; Lu, P. T.; Yu, X. F.; Zhang, W. B.; Huang, M. J.; Wu, K.; Guo, K.; Wesdemiotis, C.; Zhu, X. L.; Zhang, Z. B.; Yue, K.; Cheng, S. Z. D. Sequential "Click" Synthesis of "Nano-Diamond-Ring-like" Giant Surfactants Based on Functionalized Hydrophilic POSS/C60 Tethered with Cyclic Polystyrenes. *Macromolecules* **2014**, *47*, 4160−4168.

(22) Li, J. Z.; Zhou, Z.; Ma, L.; Chen, G. X.; Li, Q. F. Hierarchical Assembly of Amphiphilic POSS-cyclodextrin Molecules and Azobenzene End-capped Polymers. *Macromolecules* **2014**, *47*, 5739−5748.

(23) Zhang, W. A.; Yuan, J. Y.; Weiss, S.; Ye, X. D.; Li, C. L.; Müller, A. H. E. Telechelic Hybrid Poly(acrylic acid)s Containing Polyhedral Oligomeric Silsesquioxane (POSS) and Their Self-assembly in Water. *Macromolecules* **2011**, *44*, 6891−6898.

(24) Majumdar, P.; Lee, E.; Gubbins, N.; Stafslien, S. J.; Daniels, J.; Thorson, C. J.; Chisholm, B. J. Synthesis and Antimicrobial Activity of Quaternary Ammonium-functionalized POSS (Q-POSS) and Polysiloxane Coatings Containing Q-POSS. *Polymer* **2009**, *50*, 1124−1133.

(25) Li, G. Z.; Wang, L. C.; Ni, H. L.; Pittman, C. U., Jr. Polyhedral Oligomeric Silsesquioxane (POSS) Polymers and Copolymers: a Review. *J. Inorg. Organomet. Polym.* **2001**, *11*, 123−154.

(26) Wei, K.; Wang, L.; Li, L.; Zheng, S. X. Synthesis and Characterization of Bead-like Poly (N-isopropylacrylamide) Copolymers with Double Decker Silsesquioxane in the Main Chains. *Polym. Chem.* **2015**, *6*, 256−269.

(27) Minton, T. K.; Wright, M. E.; Tomczak, S. J.; Marquez, S. A.; Shen, L. H.; Brunsvold, A. L.; Cooper, R.; Zhang, J. M.; Vij, V.; Guenthner, A. J.; Petteys, B. J. Atomic Oxygen Effects on POSS Polyimides in Low Earth Orbit. *ACS Appl. Mater. Interfaces* **2012**, *4*, 492−502.

(28) Gonzalez, R. I.; Phillips, S. H.; Hoflund, G. B. In situ Oxygen-atom Erosion Study of Polyhedral Oligomeric Silsesquioxane-siloxane Copolymer. *J. Spacecr. Rockets* **2000**, *37*, 463−467.

(29) Leu, C. M.; Chang, Y. T.; Wei, K. H. Synthesis and Dielectric Properties of Polyimide-tethered Polyhedral Oligomeric Silsesquioxane (POSS) Nanocomposites via POSS-diamine. *Macromolecules* **2003**, *36*, 9122−9127.

(30) Hoflund, G. B.; Gonzalez, R. I.; Phillips, S. H. In situ Oxygen Atom Erosion Study of a Polyhedral Oligomeric Silsesquioxane-polyurethane Copolymer. *J. Adhes. Sci. Technol.* **2001**, *15*, 1199−1211.

(31) Wu, S. M.; Hayakawa, T.; Kakimoto, M. A.; Oikawa, H. Synthesis and Characterization of Organosoluble Aromatic Polyimides Containing POSS in Main Chain Derived from Double-decker-shaped Silsesquioxane. *Macromolecules* **2008**, *41*, 3481−3487.

DOI: 10.1021/acsami.5b05490
ACS Appl. Mater. Interfaces 2015, 7, 20144−20155

(32) *Standard Practices for Ground Laboratory Atomic Oxygen Interaction Evaluation of Materials for Space Applications,* ASTM E2089−00; ASTM International: West Conshohocken, PA, 2014.
(33) Atar, N.; Grossman, E.; Gouzman, I.; Bolker, A.; Murray, V. J.; Marshall, B. C.; Qian, M.; Minton, T. K.; Hanein, Y. Atomic-oxygen-durable and Electrically-conductive CNT-POSS-Polyimide Flexible Films for Space Applications. *ACS Appl. Mater. Interfaces* **2015**, *7*, 12047−12056.
(34) Watson, K. A.; Palmieri, F. L.; Connell, J. W. Space Environmentally Stable Polyimides and Copolyimides Derived from [2, 4-bis(3-aminophenoxy) phenyl] Diphenylphosphine oxide″. *Macromolecules* **2002**, *35*, 4968−4974.
(35) Verker, R.; Grossman, E.; Gouzman, I.; Eliaz, N. POSS-polyimide Nanocomposite Films: Simulated Hypervelocity Space Debris and Atomic Oxygen Effects. *High Perform. Polym.* **2008**, *20*, 475−491.
(36) Narushima, K.; Yamashita, N.; Isono, Y.; Islam, M. R.; Takeuchi, M.; Islam, M. R.; Takeuchi, M. Effect of Irradiation Power on Surface Modification of Polyester by Ammonia Plasma Treatment. *Jpn. J. Appl. Phys.* **2008**, *47*, 3603−3605.
(37) Ramires, P. A.; Mirenghi, L.; Romano, A. R.; Palumbo, F.; Nicolardi, G. Plasma-treated PET Surfaces Improve the Biocompatibility of Human Endothelial Cells. *J. Biomed. Mater. Res.* **2000**, *51*, 535−539.
(38) Kong, J.; Wang, M. J.; Zou, J. H.; An, L. N. Soluble and Meltable Hyperbranched Polyborosilazanes towards High-temperature Stable SiBCN Ceramics. *ACS Appl. Mater. Interfaces* **2015**, *7*, 6733−6744.
(39) Nakayama, Y.; Imagawa, K.; Tagashira, M.; Nakai, M.; Kudoh, H.; Sugimoto, M.; Kasai, N.; Seguchi, T. Evaluation and Analysis of Thermal Control Materials under Ground Simulation Test for Space Environment Effects. *High Perform. Polym.* **2001**, *13*, 433−451.
(40) López-Santos, C.; Yubero, F.; Cotrino, J.; González-Elipe, A. R. Surface Functionalization, Oxygen Depth Profiles, and Wetting Behavior of PET Treated with Different Nitrogen Plasmas. *ACS Appl. Mater. Interfaces* **2010**, *2*, 980−990.
(41) Edwards, D. L.; Tighe, A. P.; Eesbeek, M. V.; Kimoto, Y.; de Groh, K. K. Overview of the Natural Space Environment and ESA, JAXA, and NASA Materials Flight Experiments. *MRS Bull.* **2010**, *35*, 25−34.
(42) De Groh, K. K.; Banks, B. A.; Mccarthy, C. E.; Rucker, R. N.; Roberts, L. M.; Berger, L. A. MISSE 2 PEACE polymers atomic oxygen erosion experiment on the international space station. *High Perform. Polym.* **2008**, *20*, 388−409.
(43) Zheng, L.; Farris, R. J.; Coughlin, E. B. Novel Polyolefin Nanocomposites: Synthesis and Characterizations of Metallocene-catalyzed Polyolefin Polyhedral Oligomeric Silsesquioxane Copolymers. *Macromolecules* **2001**, *34*, 8034−8039.
(44) Liu, Y.; Shi, Z. X.; Xu, H. J.; Fang, J. H.; Ma, X. D.; Yin, J. Preparation, Characterization, and Properties of Novel Polyhedral Oligomeric Silsesquioxane-Polybenzimidazole Nanocomposites by Friedel-Crafts Reaction. *Macromolecules* **2010**, *43*, 6731−6738.
(45) Huang, J. C.; He, C. B.; Xiao, Y.; Mya, K. Y.; Dai, J.; Siow, Y. P. Polyimide/POSS Nanocomposites: Interfacial Interaction, Thermal Properties and Mechanical Properties. *Polymer* **2003**, *44*, 4491−4499.
(46) Wu, J.; Mather, P. T. POSS Polymers: Physical Properties and Biomaterials Applications. *Polym. Rev.* **2009**, *49*, 25−63.
(47) Lei, X. F.; Qiao, M. T.; Tian, L. D.; Yao, P.; Ma, Y.; Zhang, H. P.; Zhang, Q. Y. Improved Space Survivability of Polyhedral Oligomeric Silsesquioxane (POSS) Polyimides Fabricated via Novel POSS-diamine. *Corros. Sci.* **2015**, *90*, 223−238.
(48) Lei, X. F.; Chen, Y.; Zhang, H. P.; Li, X. J.; Yao, P.; Zhang, Q. Y. Space Survivable Polyimides with Excellent Optical Transparency and Self-Healing Properties Derived from Hyperbranched Polysiloxane. *ACS Appl. Mater. Interfaces* **2013**, *5*, 10207−10220.

DOI: 10.1021/acsami.5b05490
ACS Appl. Mater. Interfaces 2015, 7, 20144−20155